Check for updates

How to cite: *Angew. Chem. Int. Ed.* **2023,** *62,* e202219050
International Edition: doi.org/10.1002/anie.202219050
German Edition: doi.org/10.1002/ange.202219050

Fluorescence Imaging | Hot Paper

Reversible Live-Cell Labeling with Retro-engineered HaloTags Enables Long-Term High- and Super-Resolution Imaging

Michael Holtmannspötter, Eike Wienbeuker, Timo Dellmann, Isabelle Watrinet, Ana J. Garcia-Sáez, Kai Johnsson, Rainer Kurre, and Jacob Piehler**

Abstract: Self-labeling enzymes (SLE) such as the HaloTag have emerged as powerful tools in high and super-resolution fluorescence microscopy. Newly developed fluorogenic SLE substrates enable imaging in the presence of excess dye. To exploit this feature for reversible labeling, we engineered two variants of HaloTag7 with restored dehalogenase activity. Kinetic studies in vitro showed different turnover kinetics for reHaloTagS ($\approx 0.006\ s^{-1}$) and reHaloTagF ($\approx 0.055\ s^{-1}$). Imaging by confocal and stimulated emission depletion microscopy yielded 3-5-time enhanced photostability of reHaloTag labeling. Prominently, single molecule imaging with reHaloTags enabled controlled and stable labeling density over extended time periods. By combination with structured illumination, simultaneous visualization of single molecule diffusion and organellar dynamics was achieved. These applications highlight the potential of reHaloTag labeling for pushing the limits of advanced fluorescence microscopy techniques.

Introduction

Numerous recent discoveries in molecular cell biology have been made possible by revolutionary developments in light microscopy during the past two decades. To date, diverse fluorescence microscopy techniques are commercially available that enable imaging with a resolution far beyond the diffraction limit. In particular stimulated emission depletion (STED) and single molecule localization microscopy (SMLM) have matured into techniques that routinely achieve spatial resolution below 40 nm.[1] Even molecular resolution can be achieved as recently demonstrated by several SMLM techniques[2] such as DNA point accumulation for imaging in nanoscale topography (DNA-PAINT)[3] or minimal photon flux-based techniques (MINFLUX/MINSTED).[4] Successful application of these techniques, however, strongly depends on fluorescence labeling. In most cases, fluorescent proteins cannot provide the brightness and photostability required for super-resolution imaging below 20 nm. While labeling based on antibodies, nanobodies or other specific binders is readily achieved in fixed cells, site-specific protein labeling with synthetic chromophores in living cells has remained challenging. Self-labeling enzymes (SLE) such as the SNAP-tag[5] or the HaloTag[6] have emerged as generic tools for posttranslational fluorescence labeling in a wide variety of organisms, which have proven to be highly instrumental for the tremendous progress of diverse live cell super-resolution techniques.[7] These approaches are based on engineered enzymes, which irreversibly react with fluorophore-conjugated substrates. Further optimization of SLEs has been achieved by developing fluorogenic substrates, thus enabling wash-free labeling in living cells and organisms.[8] Under these conditions, irreversible coupling of the chromophore to the SLE is not an absolute necessity. Rather, reversible binding would allow continuous exchange of bleached chromophores, thus enabling extended time-lapse imaging, as has been previously exploited for STED microcopy,[8h,9] a technique that is severely limited by photobleaching. Likewise, elegant SMLM techniques based on reversible binding of (fluorogenic) substrates have been devised, so-called PAINT techniques.[10] Thus, reversible SLE label may open exciting possibilities for long-term time-lapse super-resolution imaging in living cells.

Here, we report reversible labeling based on the HaloTag7,[6] for which highly reactive and fluorogenic substrates have been developed.[8c,e,f,11] The HaloTag is based on the dehalogenase DhaA from *Rhodococcus sp.* that was engineered to react irreversibly with derivatives of 1-chlorohexane (HaloTag ligand, HTL).[6] To enable dissociation of the HaloTag ligand (HTL), we restored the HaloTag's dehalogenase function by reverting previous

[*] Dr. M. Holtmannspötter, E. Wienbeuker, I. Watrinet, Dr. R. Kurre, Prof. Dr. J. Piehler
Department of Biology/Chemistry and Center for Cellular Nanoanalytics, Osnabrück University
Barbarastraße 11, 49076 Osnabrück (Germany)
E-mail: michael.holtmannspoetter@uni-osnabrueck.de
piehler@uos.de
Dr. T. Dellmann, Prof. Dr. A. J. Garcia-Sáez
Institute for Genetics and Cologne Excellence Cluster on Cellular Stress Responses in Aging-Associated Diseases (CECAD), University of Cologne
Joseph-Stelzmann-Straße 26, 50931 Cologne (Germany)
Prof. Dr. K. Johnsson
Department of Chemical Biology, Max Planck Institute for Medical Research
Jahnstraße 29, 69120 Heidelberg (Germany)

© 2023 The Authors. Angewandte Chemie International Edition published by Wiley-VCH GmbH. This is an open access article under the terms of the Creative Commons Attribution License, which permits use, distribution and reproduction in any medium, provided the original work is properly cited.

© 2023 The Authors. Angewandte Chemie International Edition published by Wiley-VCH GmbH

mutations in the catalytic site (Figure 1A, B). We generated two HaloTag variants, reHaloTagS and reHaloTagF, which reversibly bind fluorescent HTL derivatives with turnover kinetics in the seconds-to-minutes regime. We demonstrate the application of reHaloTag labeling to achieve prolonged time-lapse imaging by diverse advanced and super-resolution microscopy techniques with features that are particularly powerful for single molecule tracking and localization microscopy (TALM).

Results and Discussion

Efficient, yet reversible binding of HaloTag ligands to reHaloTag variants

The HaloTag was engineered to irreversibly bind a synthetic chloroalkane substrate, the HaloTag ligand (HTL), forming an ester with a nucleophilic Asp residue at position 106 (Figure 1A).[6] To achieve reversible HTL binding, we restored the dehalogenase activity by mutating Asn272 of HaloTag7 into His, which catalyzes the hydrolysis of the ester formed by Asp106 and the substrate (HaloTag7N272H, "reHaloTagS"). In a second variant, we combined this mutation with restoring the adjacent Leu273 back into a Tyr (HaloTag7N272H/L273Y, "reHaloTagF"). In the active dehalogenase, Tyr273 directly contacts His272, and therefore may be important for its proper positioning. We assumed that these reversible binding HaloTag (reHaloTag) variants would allow exchange of photobleached dye by promoting hydrolysis of the ester bond (Figure 1B) and thus enable prolonged time-lapse imaging.

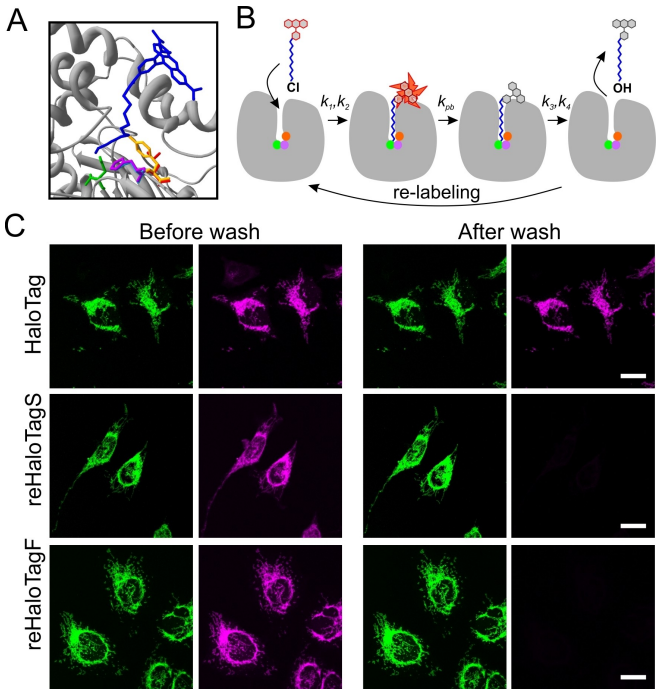

Figure 1. Reversible labeling of retro-engineered HaloTag variants. (A) Overlay of the HaloTag with the substrate HTL-TMR (blue) covalently bound to D106 (green) and the original dehalogenase DhaA (pdb: 6U32 and 1BN7, respectively). In addition, the side chains of the catalytic H272 (magenta) and the adjacent Y273 (orange) restored in the reHaloTags are shown. All numbers refer to the HaloTag7 sequence. (B) Concept of reversible labeling exploiting catalytically active reHaloTags. (C) Reversible labeling of mEGFP-Tom20 fused to different variants of the HaloTag. HeLa cells stably transfected with these constructs were fixed and imaged in presence of 250 nM HTL-MaP555 (magenta) with the GFP signal as a control (green). Cells were additionally imaged after washing out the substrate. Scale bar: 20 µm.

For proof-of-concept experiments, we tested labeling of different HaloTag variants in fixed cells. To validate labeling specificity, the translocase in the outer mitochondrial membrane (OMM) subunit Tom20, fused to mEGFP and the different versions of the HaloTag was used as a target. These variants were stably expressed in HeLa cells, fixed with paraformaldehyde and then imaged by confocal laser scanning microscopy (cLSM) in the presence of the fluorogenic substrate HTL-MaP555. Similar signal intensities for all three variants perfectly overlaying with the GFP channel were obtained, highlighting that the mutations did not compromise the HaloTag's ability to react with the substrate (Figure 1C). Upon washing out the substrate, labeling of Tom20-mEGFP-HaloTag remained at a largely identical level as before. By contrast, the signal in the MaP555 channel was almost entirely gone in cells expressing Tom20 fused to reHaloTagS and reHaloTagF, respectively (Figure 1C), with $\leq 5\,\%$ intensity remaining. Very similar behavior was observed in living cells, confirming efficient, yet reversible labeling by the engineered reHaloTag variants (Supplementary Figure S1A).

We further explored the capabilities of the reHaloTag variants by sequential labeling with two different fluorogenic substrates (HTL-MaP555 and HTL-MaP618). To this end, fixed HeLa cells expressing Tom20-mEGFP fused to one of the different HaloTag variants were first stained with 200 nM HTL-MaP555. After the initial frame, 800 nM HTL-MaP618 was added to the microscopy chamber. For the HaloTag7, only a slight fluorescence increase in the MaP618 channel was observed, which was largely at the level of unspecific background (Supplementary Figure S1B). In turn, the MaP555 signal remained almost unchanged with a decrease largely caused by photobleaching. In contrast, efficient exchange of HTL-MaP555 by HTL-MaP618 was observed for the reHaloTags (Supplementary Figure S1). Interestingly, we could see that this exchange was substantially faster for reHaloTagF as compared to reHaloTagS. Thus, these experiments not only confirmed reversible labeling but also suggested different turnover kinetics of the reHaloTag variants.

Differential exchange kinetics of reHaloTagS and reHaloTagF

We therefore quantified the substrate exchange kinetics of the reHaloTag proteins more precisely by fluorescence recovery after photobleaching (FRAP). These experiments were carried out using the same HeLa cell lines stably expressing Tom20-mEGFP fused to one of the three different HaloTag variants. After fixation, FRAP experiments

© 2023 The Authors. Angewandte Chemie International Edition published by Wiley-VCH GmbH

15213773, 2023, 18, Downloaded from https://onlinelibrary.wiley.com/doi/10.1002/anie.202219050 by MPI 302 Biophysics, Wiley Online Library on [01/12/2023]. See the Terms and Conditions (https://onlinelibrary.wiley.com/terms-and-conditions) on Wiley Online Library for rules of use; OA articles are governed by the applicable Creative Commons License

were carried out in the presence of 250 nM HTL-MaP555. As expected, significant FRAP was observed only for the reHaloTags, but not for HaloTag7 (Figure 2A). FRAP curves for reHaloTagS and reHaloTagF, however, confirmed very different exchange kinetics (Figure 2B) with rate constants $k_{ex} = (5.7 \pm 0.1) \times 10^{-3}\ s^{-1}$ and $k_{ex} = (55 \pm 18) \times 10^{-3}\ s^{-1}$, respectively. Surprisingly, the exchange rate constants did hardly change upon increasing the temperature from room temperature (≈25 °C) to 37 °C (Figure 2B and Table 1).

The reaction cycle of dehalogenases has been described by a 4-step kinetic model[12] with the rate constants k_1 and k_2 determining substrate association and ester bond formation, respectively, and the rate constants k_3 and k_4 determining ester hydrolysis and product dissociation (cf. Figure 1B). Given the high rate constants of fluorescent HTL substrates reacting with HaloTag7,[13] we expect the exchange kinetics to be limited by k_3 and/or k_4 at the high substrate concentrations used during the FRAP experiments. To independently verify this assumption and to quantify the kinetics more reliably, we probed the reaction of fluorogenic substrates with immobilized reHaloTag by simultaneous total internal reflection fluorescence spectroscopy and reflectance interferometry (TIRFS-RIf) in a flow through system.[14] For this purpose, recombinant HaloTag and reHaloTag proteins fused to a His-tag were immobilized onto a transducer slide functionalized with tris-NTA.[15] Upon injection of HTL-JF549, rapid binding to all variants was observed reaching similar binding levels with rather similar kinetics (Figure 2C and Supplementary Figure S3) with an overall mean on-rate constant k_{on} of $\approx 1.7 \times 10^6\ M^{-1} s^{-1}$ (Table 1). Upon washing out the substrate, however, very different dissociation kinetics were observed: while the fluorescence remained constant for HaloTag7, complete decay was observed for the reHaloTag proteins with apparent dissociation rate constants $k_{off} = (4.9 \pm 0.4) \times 10^{-3}\ s^{-1}$ for reHaloTagS and $k_{off} = (73 \pm 3) \times 10^{-3}\ s^{-1}$ for reHaloTagF. These numbers are very much in line with the rate constants observed in FRAP experiments, confirming the ≈10-fold different turnover kinetics of reHaloTagS and reHaloTagF. While we anticipate that the exchange kinetics is largely determined by the rate constant of ester hydrolysis (k_3, cf. Figure 1B), we cannot rule out that also dissociation of the products from the binding pocket (k_4) may be rate limiting.[12b] The L273Y mutation of reHaloTagF may affect either or both, catalytic activity and binding of the product.

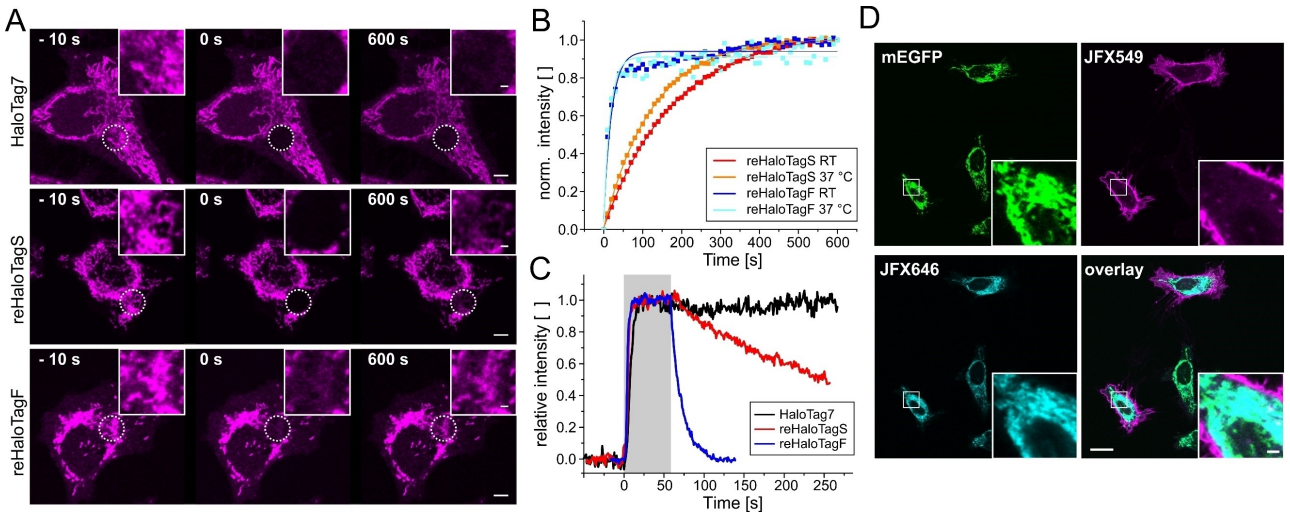

Figure 2. Differential exchange kinetics of reHaloTag variants. (A) Exchange kinetics probed by FRAP at room temperature: HeLa cells stably expressing Tom20 fused to different HaloTag variant were fixed and imaged in the presence of 250 nM HTL-MaP555, followed by FRAP in a circular ROI (outlined by the dotted lines and enlarged in the insets). Scale bar: 5 μm (inset: 1 μm). (B) Comparison of the recovery kinetics for reHaloTagS and reHaloTagF at different temperatures. (C) In vitro kinetics of HTL-JF549 reacting with immobilized HaloTag variants (HaloTag7, black; reHaloTagS, red; reHaloTagF, blue) monitored by TIRF spectroscopy. The grey bar marks the injection period. Curves were normalized to the equilibrium intensity reached during injection. (D) Orthogonal dual-color labeling of HaloTag and reHaloTagF in living cells. HeLa cells stably expressing Tom20-mEGFP-reHaloTagF were transiently transfected with HaloTag7 fused to a transmembrane domain targeted to the plasma membrane and sequentially labeled with HTL-JFX549 and HTL-JFX646. Scale bar: 20 μm (inset: 2 μm).

Table 1: Enzymatic rate constants observed for different HaloTag variants.

Variant	k_{on} (k_1, k_2)[a] [$10^6\ M^{-1} s^{-1}$]	k_{off} (k_3, k_4)[a] [$10^{-3}\ s^{-1}$]	K_{eq}[b] [nM]	k_{ex} (RT)[c] [$10^{-3}\ s^{-1}$]	k_{ex} (37 °C)[c] [$10^{-3}\ s^{-1}$]
HaloTag7	1.8 ± 0.6	–	–	–	–
reHaloTagS	2.4 ± 0.2	4.9 ± 0.4	2.1 ± 0.3	5.7 ± 0.1	8.1 ± 0.1
reHaloTagF	1.1 ± 0.2	73 ± 3	66 ± 7	55 ± 18	67 ± 26

[a] From TIRFS binding assays. [b] Calculated from k_{off}/k_{on}. [c] From FRAP experiments in fixed cells.

© 2023 The Authors. Angewandte Chemie International Edition published by Wiley-VCH GmbH

15213773, 2023, 18, Downloaded from https://onlinelibrary.wiley.com/doi/10.1002/anie.202219050 by MPI 302 Biophysics, Wiley Online Library on [01/12/2023]. See the Terms and Conditions (https://onlinelibrary.wiley.com/terms-and-conditions) on Wiley Online Library for rules of use; OA articles are governed by the applicable Creative Commons License

Dual-color labeling by combining reversible and irreversible HaloTags

Reversible and irreversible reaction with different HaloTag variants opens the possibility for orthogonal dual-color labeling of two different proteins. To test this opportunity, HeLa cells stably expressing Tom20-mEGFP-reHaloTagF were transiently transfected with HaloTag7 fused to a transmembrane domain targeted to the plasma membrane (HaloTag-TMD) to ensure a clearly distinguishable subcellular localization.

To achieve orthogonality, live cells were sequentially incubated with 50 nM HTL-JFX549, washed and then imaged in the presence of 200 nM HTL-JFX646. While in the first step both HaloTag variants were labeled with HTL-JFX549, only HaloTag7 remained labeled after washout (Supplementary Figure S2). Thus, orthogonal labeling of reHaloTagF and HaloTag7 was observed when adding HTL-JFX646 in the last step of the labeling procedure (Figure 2D).

reHaloTags increase the apparent photostability in confocal and STED microscopy

Having generated reHaloTag variants capable to exchange fluorophores in the seconds-to-minutes time regimes, we further explored their capabilities in time-lapse imaging by high- and super-resolution confocal microscopy techniques. In Figure S4A, live cell time-lapse confocal imaging of Tom20 tagged with different HaloTag variants over the time course of 20 min at a time resolution of 10 s is compared (cf. Supplementary Movie S1). Experiments were performed in the presence of HTL-MaP555 and at a constant excitation power that ensured significant photobleaching while avoiding photostress for the cells. Strikingly, substantially reduced photobleaching was observed for the reHaloTag variants as compared to HaloTag7, with the reHaloTagF outperforming the reHaloTagS. Overall, a >5-fold enhanced apparent photostability of reHaloTagF compared to HaloTag7 was estimated based on mono-exponential fitting of the decay curves (Figure 3A, Figure S4A and Supporting Information Table S1). The substantial loss of fluorescence even in the case of freely exchangeable substrate, however, implicates that photobleaching of the dye can lead to photodamage of the reHaloTag's enzymatic function.

Similar performance of reHaloTag labeling was observed in STED microscopy experiments. As STED super-resolution is based on spatially controlled reversible de-excitation of fluorophores at very strong light intensities, typically organic dyes with high quantum yield and utmost photostability are required. Although high-performance dyes are available, time-lapse STED of living cells at low signal levels is still limited by photobleaching and, therefore, remains challenging.[16] We therefore compared imaging of Tom20 fused to different HaloTag variants in live HeLa cells by STED microscopy. Under these conditions, the OMM in all three Tom20-mEGFP-HaloTag variants could be nicely resolved (Figure 3B and Supplementary Movie S2). Time-lapse STED imaging with a 1 min time interval yielded strong decrease in fluorescence intensities for the HaloTag7, and only a mild improvement was observed for reHaloTagS (Figure 3B, C). By contrast, labeling via reHaloTagF considerably reduced photobleaching. Given a multiexponential photobleaching kinetics observed in these experiments (Supporting Information Table S2), only semi-quantitative comparison was possible. Overall, confocal and STED imaging results highlight that at these relatively fast time-lapse imaging conditions, faster exchange rates of the reHaloTagF are beneficial to minimize photobleaching resulting in a prolonged STED imaging and the important possibility to use higher frame rates.

Prolonged tracking and localization microscopy with stable molecule density

We have previously introduced single molecule tracking and localization microscopy (TALM) as a powerful approach to visualize and quantify the morphology and dynamics of organellar microcompartments.[17] This approach is often based on substoichiometric labeling and SLE have proven highly useful to reduce labeling density.[7c,18] However, controlling labeling density by an irreversible reaction is not

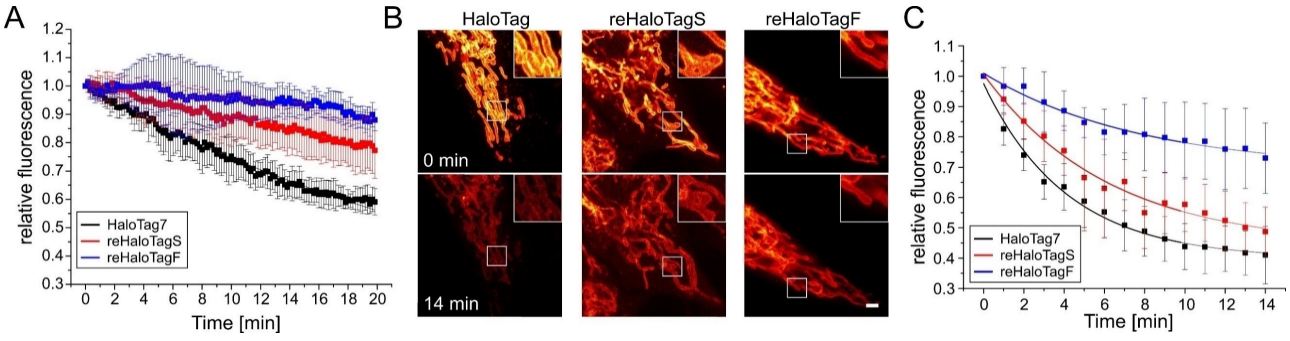

Figure 3. Prolonged time-lapse confocal and STED microscopy. (A) Decay of the fluorescence intensity during confocal imaging compared for the different variants. (B) Live cell STED imaging of Tom20 in HeLa cells using labeling of different HaloTag variants. Imaging in presence of 1 μM HTL-MaP555. Insets show exemplary regions underlining the bleaching differences between each variant. Scale bar: 2 μm (C) Decay of the fluorescence intensity during STED imaging compared for the different variants.

© 2023 The Authors. Angewandte Chemie International Edition published by Wiley-VCH GmbH

15213773, 2023, 18, Downloaded from https://onlinelibrary.wiley.com/doi/10.1002/anie.202219050 by MPI 302 Biophysics, Wiley Online Library on [01/12/2023]. See the Terms and Conditions (https://onlinelibrary.wiley.com/terms-and-conditions) on Wiley Online Library for rules of use; OA articles are governed by the applicable Creative Commons License

trivial, as the reaction needs to be stopped at the right moment or finally tuned by controlled photobleaching, which in turn leads to phototoxicity and cell stress. Moreover, the major fraction of target molecules remains unlabeled and thus does not contribute information. We therefore explored, to what extend these disadvantages are effectively overcome by reHaloTag labeling. For single molecule imaging, HeLa cells expressing Tom20 tagged with one of the different HaloTag variants were imaged in highly inclined laminar optical sheet (HILO) mode with a time resolution of 30 fps. To ensure low labeling density, we applied 500 pM HTL-MaP555 and imaged in the presence of substrate. In case of HaloTag7, substantial photobleaching was required to reach densities suitable for single molecule localization (Supplementary Movie S3). Therefore, reliable TALM analysis was only possible about 100 s (3000 frames) after starting image acquisition (Figure 4A). By contrast, much more robust single molecule densities were observed for reHaloTagS and reHaloTagF (Figure 4B, C and Supplementary Movie S4, S5). Thus, high-quality super-resolution images could be generated over the entire course of the 12 min imaging experiment (Figure 4A–C). The fundamental improvement achieved for TALM imaging by reHaloTag labeling is highlighted by comparing how the number of localized molecules changes over time (Figure 4D). In case of HaloTag7, the kinetics is largely determined by reversible photoswitching[7b] in combination with some irreversible photobleaching, yielding a biphasic decay. A quasi-stable level of molecules that could be reliably localized was only reached after 300 s at a level of $<10\,\%$ of the initial density. By contrast, the photochemical kinetics of the reHaloTag variants is convolved with the exchange kinetics, resulting into quasi-steady-state levels of single molecule densities at much faster times and relatively high levels as compared to the initial density. For reHaloTagF, this stable state was reached after less than 30 s, and less than 15 % further decrease in the molecule density was observed in the subsequent 10 min acquisition time (18000 frames). Faster exchange kinetics, however, does not compromise tracking fidelity as confirmed by comparison of the trajectory length histograms over time and diffusion coefficients for the three HaloTag variants (Figure 4E, Supplementary Figure S5). Interestingly, reHaloTags even showed somewhat more robust trajectory length's over time as compared to the HaloTag7 (Figure 4E). These results highlight that the moderate exchange kinetics of reHaloTag variants enable powerful control of labeling density without compromising tracking fidelity, and thus have particular potential for application in single molecule microscopy techniques, especially long-term TALM imaging.

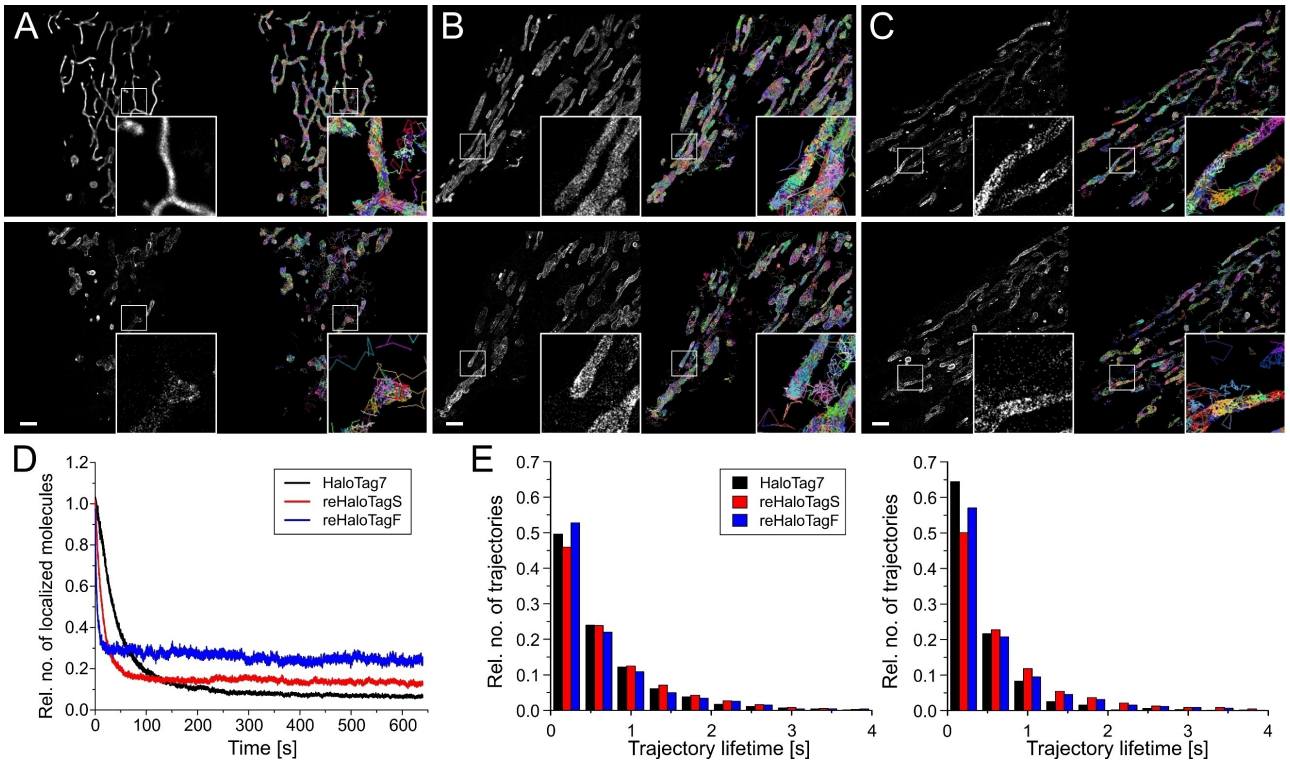

Figure 4. reHaloTag labeling ensures robust single molecule density for long-term TALM imaging. (A–C) Single molecule localization (left panels) and single molecule trajectories from time-lapse imaging of Tom20 in Hela cells using labeling of different HaloTag variants (right panels). Images rendered from frames 1-2000 (top) and 18001–20000 (bottom). Insets show zoom into representative regions. Imaging was carried out in the presence of 500 pM HTL-MaP555. Scale bars: 2 µm. (D) Comparison of the relative number of localized molecules over the entire time span. (E) Trajectory length histograms obtained the corresponding time windows: 1–2000 (left), and 18001–20000 (right).

© 2023 The Authors. Angewandte Chemie International Edition published by Wiley-VCH GmbH

15213773, 2023, 18, Downloaded from https://onlinelibrary.wiley.com/doi/10.1002/anie.202219050 by MPI 302 Biophysics, Wiley Online Library on [01/12/2023]. See the Terms and Conditions (https://onlinelibrary.wiley.com/terms-and-conditions) on Wiley Online Library for rules of use; OA articles are governed by the applicable Creative Commons License

reHaloTags enable simultaneous SIM and TALM

Exploiting their unique capability to control steady state labeling, we further pushed the application of the two reHaloTag variants by using dual-color labeling for simultaneous ensemble and single molecule microscopy. For this purpose, we combined single-molecule imaging with super-resolution structured illumination microscopy (SIM). HeLa cells expressing Tom20-mEGFP-reHaloTagF were labeled by mixing 250 nM HTL-MaP555 for SIM acquisition and 500 pM HTL-JFX646 for single molecule localization. Imaging was performed by alternating acquisition of nine SIM images in the MaP555 channel followed by acquisition of 84 frames in the JFX-646 channel for TALM. Under these conditions, the OMM could be well resolved by SIM to visualize mitochondrial dynamics beyond the diffraction limit (Figure 5A, Supplementary Movie S6). These images could be correlated with the diffusion of Tom20 resolved at single molecule level. Importantly, reorganization of the OMM network by fusion and fission could be monitored by SIM (but not TALM), which in turn can explain changes in the confinement observed in single molecule trajectories (Figure 5B and Supplementary Movie S7). The relatively fast exchange kinetics of the reHaloTagF enabled long-term correlative SIM and robust TALM imaging at the same time.

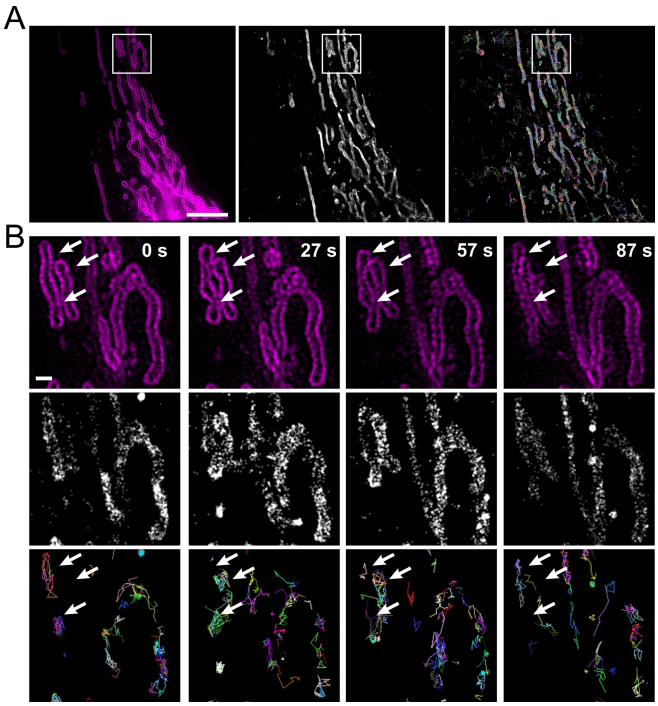

Figure 5. Simultaneous structured illumination (SIM) and single molecule tracking and localization microscopy (TALM). (A) Imaging of HeLa cells expressing Tom20-mEGFP-reHaloTagF in the presence of 250 nM HTL-MaP555 for SIM acquisition and 500 pM HTL-JFX646 for single molecule imaging. Representative SIM image (magenta), reconstruction of single molecule localizations of 2759 frames (gray) and the corresponding trajectories. Scale bar: 5 μm (B) Time-lapse SIM imaging (top), cumulative TALM (middle) and single molecule trajectories (bottom) of the ROIs shown in A. Arrows indicate regions showing transient fission and fusion of the OMM and thus changes in the confinement of single molecule trajectories. Top. Scale bar: 1 μm.

Conclusion

Application of advanced and super-resolution imaging techniques in living cells are still limited by photostability of fluorescent labels. Here, we have introduced reversible HaloTag (reHaloTag) labeling as a novel tool to increase the resistance against photobleaching and to control post-translational labeling density for single molecule imaging. By restoring the original dehalogenase capabilities of HaloTag7, we obtained reHaloTagS and reHaloTagF with a ≈10-fold difference in the exchange rate constant. Both reHaloTag variants proved suitable to enhance apparent photostability in different high- and super-resolution imaging techniques such as cLSM, STED, SIM and TALM, with the reHaloTagF showing overall superior features in our applications. However, the suitability of each variant likely depends on the time resolution required, and here we focused on fast imaging applications that benefit from high turnover kinetics. We tested four HTL derivatives, yielding very similar results with respect to labeling efficiency and turnover kinetics. We therefore expect that most available HaloTag substrates are compatible with our approach and thus a broad spectrum of fluorogenic variants[8] can be exploited. However, a significant contribution of the conjugated moiety for the on-rate has been reported for HTL substrates[13] and therefore some minor differences in labeling efficiencies can be expected. The availability of different substrates furthermore opened the possibility for orthogonal labeling of HaloTag7 and reHaloTagF. At the downside, reHaloTags degrade their substrates and therefore, reduced labeling due to depletion of the substrate can be expected upon long-term application in samples with high total quantities of the reHaloTags.

With these features, reHaloTag-based labeling nicely complements the recently developed non-covalent HaloTag ligands (xHTLs).[19] These xHTLs bind substantially more transiently, with complex lifetimes in the milliseconds to second's regime, compared to the 15–200 s observed for the reHaloTag system. The longer lifetimes and resulting higher affinities of reHaloTag variants compared to the xHTL system can potentially ensure higher signal-to-background in ensemble measurements as well as higher tracking fidelity in single molecule imaging approaches. In turn, xHTLs open unique possibilities for PAINT due to their transient nature that is comparable to the unbinding kinetics used in DNA-PAINT.

While we found improved performance of reHaloTag labeling in all fluorescence microscopy techniques we tested, the approach appears particularly useful for single molecule tracking and localization microscopy (TALM). Here, the ability to control labeling density at very low substrate concentrations in conjunction with the relatively long lifetime of the substrate bound to the reHaloTags proved ideal. For single molecule dynamics, the lifetime of the reHalo-

© 2023 The Authors. Angewandte Chemie International Edition published by Wiley-VCH GmbH

15213773, 2023, 18, Downloaded from https://onlinelibrary.wiley.com/doi/10.1002/anie.202219050 by MPI 302 Biophysics, Wiley Online Library on [01/12/2023]. See the Terms and Conditions (https://onlinelibrary.wiley.com/terms-and-conditions) on Wiley Online Library for rules of use; OA articles are governed by the applicable Creative Commons License

TagF-HTL complex (≈15 s) is sufficient to ensure unbiased tracking and mobility analyses, whereas the lower lifetime of HaloTag-xHTL complexes (≈1 s) may limit the trajectory length. Combination of reHaloTag labeling with reversibly photoswitching HTL dyes[8f] may further enhance the capabilities of long-term TALM imaging.

Another striking application enabled by the well-defined exchange kinetics is the combination of ensemble and single molecule imaging using spectrally separable fluorescent substrates. The dynamic exchange of labels furthermore ensures thorough sampling of the entire population at single molecule level while continuously monitoring the overall distribution of the target protein in the cell. Here, we demonstrated super-resolution at ensemble and single molecule level by combing SIM and SMT that, given the fluorogenic nature of the substrate, can be readily extended to three-dimensional imaging. Simultaneous application of these complementary techniques opens new possibilities for correlative diffusion analyses. However, other combinations such as STED with STED-FCS or MINFLUX can be anticipated, which would similarly gain from the versatile control of labeling densities and the longer complex lifetime as compared to xHTL labeling.

Experimental Section

Materials and methods are described in detail in the Supporting Information.

Acknowledgements

We thank W. Kohl and A. Budke-Gieseking (Osnabrück University) and C. Jüngst (CECAD, University Cologne) for technical support, and Janelia Materials for providing HTL-JFX549 and HTL-JFX646. This project was supported by funding to J.P. and R.K. from the DFG (SFB 944, projects P8 and Z, PI405/10-1 and the DFG Facility iBiOs, PI 405/14-1). Open Access funding enabled and organized by Projekt DEAL.

Conflict of Interest

The authors declare no conflict of interest.

Data Availability Statement

The data that support the findings of this study are available from the corresponding author upon reasonable request.

Keywords: Fluorescent Probes · Protein Engineering · STED Microscopy · Self-Labeling Enzyme · Single Molecule Tracking

[1] a) S. J. Sahl, S. W. Hell, S. Jakobs, *Nat. Rev. Mol. Cell Biol.* **2017**, *18*, 685–701; b) Y. M. Sigal, R. Zhou, X. Zhuang, *Science* **2018**, *361*, 880–887.

[2] a) S. Liu, P. Hoess, J. Ries, *Annu. Rev. Biophys.* **2022**, *51*, 301–326; b) M. Lelek, M. T. Gyparaki, G. Beliu, F. Schueder, J. Griffie, S. Manley, R. Jungmann, M. Sauer, M. Lakadamyali, C. Zimmer, *Nat. Rev. Methods Primers* **2021**, *1*, 39.

[3] J. Schnitzbauer, M. T. Strauss, T. Schlichthaerle, F. Schueder, R. Jungmann, *Nat. Protoc.* **2017**, *12*, 1198–1228.

[4] a) K. C. Gwosch, J. K. Pape, F. Balzarotti, P. Hoess, J. Ellenberg, J. Ries, S. W. Hell, *Nat. Methods* **2020**, *17*, 217–224; b) M. Weber, M. Leutenegger, S. Stoldt, S. Jakobs, T. S. Mihaila, A. N. Butkevich, S. W. Hell, *Nat. Photonics* **2021**, *15*, 361–366; c) M. Weber, H. von der Emde, M. Leutenegger, P. Gunkel, S. Sambandan, T. A. Khan, J. Keller-Findeisen, V. C. Cordes, S. W. Hell, *Nat. Biotechnol.* **2022**, https://doi.org/10.1038/s41587-022-01519-4.

[5] A. Gautier, A. Juillerat, C. Heinis, I. R. Correa Jr., M. Kindermann, F. Beaufils, K. Johnsson, *Chem. Biol.* **2008**, *15*, 128–136.

[6] G. V. Los, L. P. Encell, M. G. McDougall, D. D. Hartzell, N. Karassina, C. Zimprich, M. G. Wood, R. Learish, R. F. Ohana, M. Urh, D. Simpson, J. Mendez, K. Zimmerman, P. Otto, G. Vidugiris, J. Zhu, A. Darzins, D. H. Klaubert, R. F. Bulleit, K. V. Wood, *ACS Chem. Biol.* **2008**, *3*, 373–382.

[7] a) B. Hein, K. I. Willig, C. A. Wurm, V. Westphal, S. Jakobs, S. W. Hell, *Biophys. J.* **2010**, *98*, 158–163; b) T. Klein, A. Loschberger, S. Proppert, S. Wolter, S. van de Linde, M. Sauer, *Nat. Methods* **2011**, *8*, 7–9; c) T. Appelhans, C. P. Richter, V. Wilkens, S. T. Hess, J. Piehler, K. B. Busch, *Nano Lett.* **2012**, *12*, 610–616; d) S. Wilmes, M. Staufenbiel, D. Lisse, C. P. Richter, O. Beutel, K. B. Busch, S. T. Hess, J. Piehler, *Angew. Chem. Int. Ed.* **2012**, *51*, 4868–4871; *Angew. Chem.* **2012**, *124*, 4952–4955; e) D. Janning, M. Igaev, F. Sundermann, J. Bruhmann, O. Beutel, J. J. Heinisch, L. Bakota, J. Piehler, W. Junge, R. Brandt, *Mol. Biol. Cell* **2014**, *25*, 3541–3551; f) B. Barlag, O. Beutel, D. Janning, F. Czarniak, C. P. Richter, C. Kommnick, V. Goser, R. Kurre, F. Fabiani, M. Erhardt, J. Piehler, M. Hensel, *Sci. Rep.* **2016**, *6*, 31601; g) C. Lang, J. Schulze, R. R. Mendel, R. Hansch, *J. Exp. Bot.* **2006**, *57*, 2985–2992; h) B. Niewidok, M. Igaev, A. Pereira da Graca, A. Strassner, C. Lenzen, C. P. Richter, J. Piehler, R. Kurre, R. Brandt, *J. Cell Biol.* **2018**, *217*, 1303–1318; i) T. Schlichthaerle, M. T. Strauss, F. Schueder, A. Auer, B. Nijmeijer, M. Kueblbeck, V. Jimenez Sabinina, J. V. Thevathasan, J. Ries, J. Ellenberg, R. Jungmann, *Angew. Chem. Int. Ed.* **2019**, *58*, 13004–13008; *Angew. Chem.* **2019**, *131*, 13138–13142.

[8] a) E. Prifti, L. Reymond, M. Umebayashi, R. Hovius, H. Riezman, K. Johnsson, *ACS Chem. Biol.* **2014**, *9*, 606–612; b) A. N. Butkevich, G. Y. Mitronova, S. C. Sidenstein, J. L. Klocke, D. Kamin, D. N. Meineke, E. D'Este, P. T. Kraemer, J. G. Danzl, V. N. Belov, S. W. Hell, *Angew. Chem. Int. Ed.* **2016**, *55*, 3290–3294; *Angew. Chem.* **2016**, *128*, 3350–3355; c) G. Lukinavicius, L. Reymond, K. Umezawa, O. Sallin, E. D'Este, F. Gottfert, H. Ta, S. W. Hell, Y. Urano, K. Johnsson, *J. Am. Chem. Soc.* **2016**, *138*, 9365–9368; d) Y. Liu, K. Miao, N. P. Dunham, H. Liu, M. Fares, A. K. Boal, X. Li, X. Zhang, *Biochemistry* **2017**, *56*, 1585–1595; e) L. Wang, M. Tran, E. D'Este, J. Roberti, B. Koch, L. Xue, K. Johnsson, *Nat. Chem.* **2020**, *12*, 165–172; f) Q. Zheng, A. X. Ayala, I. Chung, A. V. Weigel, A. Ranjan, N. Falco, J. B. Grimm, A. N. Tkachuk, C. Wu, J. Lippincott-Schwartz, R. H. Singer, L. D. Lavis, *ACS Cent. Sci.* **2019**, *5*, 1602–1613; g) P. Werther, K. Yserentant, F. Braun, K. Grussmayer, V. Navikas, M. Yu, Z. Zhang, M. J. Ziegler, C. Mayer, A. J. Gralak, M. Busch, W. Chi, F. Rominger, A. Radenovic, X. Liu, E. A. Lemke, T. Buckup, D. P. Herten, R. Wombacher, *ACS Cent. Sci.* **2021**, *7*, 1561–1571; h) M. Glogger, D. Wang, J. Kompa, A. Balakrishnan, J. Hiblot, H. D. Barth, K. Johnsson, M. Heilemann, *ACS Nano* **2022**, *16*, 17991–17997.

© 2023 The Authors. Angewandte Chemie International Edition published by Wiley-VCH GmbH

15213773, 2023, 18, Downloaded from https://onlinelibrary.wiley.com/doi/10.1002/anie.202219050 by MPI 302 Biophysics, Wiley Online Library on [01/12/2023]. See the Terms and Conditions (https://onlinelibrary.wiley.com/terms-and-conditions) on Wiley Online Library for rules of use; OA articles are governed by the applicable Creative Commons License

[9] a) J. A. Fitzpatrick, Q. Yan, J. J. Sieber, M. Dyba, U. Schwarz, C. Szent-Gyorgyi, C. A. Woolford, P. B. Berget, A. S. Waggoner, M. P. Bruchez, *Bioconjugate Chem.* **2009**, *20*, 1843–1847; b) C. Spahn, J. B. Grimm, L. D. Lavis, M. Lampe, M. Heilemann, *Nano Lett.* **2019**, *19*, 500–505.

[10] a) N. G. Bozhanova, M. S. Baranov, N. V. Klementieva, K. S. Sarkisyan, A. S. Gavrikov, I. V. Yampolsky, E. V. Zagaynova, S. A. Lukyanov, K. A. Lukyanov, A. S. Mishin, *Chem. Sci.* **2017**, *8*, 7138–7142; b) R. Jungmann, C. Steinhauer, M. Scheible, A. Kuzyk, P. Tinnefeld, F. C. Simmel, *Nano Lett.* **2010**, *10*, 4756–4761; c) G. Giannone, E. Hosy, F. Levet, A. Constals, K. Schulze, A. I. Sobolevsky, M. P. Rosconi, E. Gouaux, R. Tampe, D. Choquet, L. Cognet, *Biophys. J.* **2010**, *99*, 1303–1310; d) P. Winckler, L. Lartigue, G. Giannone, F. De Giorgi, F. Ichas, J. B. Sibarita, B. Lounis, L. Cognet, *Sci. Rep.* **2013**, *3*, 2387; e) J. Molle, M. Raab, S. Holzmeister, D. Schmitt-Monreal, D. Grohmann, Z. He, P. Tinnefeld, *Curr. Opin. Biotechnol.* **2016**, *39*, 8–16.

[11] N. Lardon, L. Wang, A. Tschanz, P. Hoess, M. Tran, E. D'Este, J. Ries, K. Johnsson, *J. Am. Chem. Soc.* **2021**, *143*, 14592–14600.

[12] a) T. Bosma, M. G. Pikkemaat, J. Kingma, J. Dijk, D. B. Janssen, *Biochemistry* **2003**, *42*, 8047–8053; b) J. P. Schanstra, J. Kingma, D. B. Janssen, *J. Biol. Chem.* **1996**, *271*, 14747–14753.

[13] a) D. Lisse, V. Wilkens, C. You, K. Busch, J. Piehler, *Angew. Chem. Int. Ed.* **2011**, *50*, 9352–9355; *Angew. Chem.* **2011**, *123*, 9524–9527; b) J. Wilhelm, S. Kuhn, M. Tarnawski, G. Gotthard, J. Tunnermann, T. Tanzer, J. Karpenko, N. Mertes, L. Xue, U. Uhrig, J. Reinstein, J. Hiblot, K. Johnsson, *Biochemistry* **2021**, *60*, 2560–2575.

[14] M. Gavutis, S. Lata, P. Lamken, P. Müller, J. Piehler, *Biophys. J.* **2005**, *88*, 4289–4302.

[15] S. Lata, J. Piehler, *Anal. Chem.* **2005**, *77*, 1096–1105.

[16] J. Oracz, V. Westphal, C. Radzewicz, S. J. Sahl, S. W. Hell, *Sci. Rep.* **2017**, *7*, 11354.

[17] a) T. Appelhans, K. Busch, *Methods Mol. Biol.* **2017**, *1567*, 273–291; b) T. Appelhans, F. R. M. Beinlich, C. P. Richter, R. Kurre, K. B. Busch, *J. Vis. Exp.* **2018**, e57690; c) T. Appelhans, K. B. Busch, *Biophys. Rev.* **2017**, *9*, 345–352.

[18] F. R. Beinlich, C. Drees, J. Piehler, K. B. Busch, *ACS Chem. Biol.* **2015**, *10*, 1970–1976.

[19] J. Kompa, J. Bruins, M. Glogger, J. Wilhelm, M. S. Frei, M. Tarnawski, E. D'Este, M. Heilemann, J. Hiblot, K. Johnsson, *J. Am. Chem. Soc.* **2023**, *145*, 3075–3083.

Manuscript received: December 23, 2022
Accepted manuscript online: February 3, 2023
Version of record online: March 10, 2023

© 2023 The Authors. Angewandte Chemie International Edition published by Wiley-VCH GmbH

15213773, 2023, 18, Downloaded from https://onlinelibrary.wiley.com/doi/10.1002/anie.202219050 by MPI 302 Biophysics, Wiley Online Library on [01/12/2023]. See the Terms and Conditions (https://onlinelibrary.wiley.com/terms-and-conditions) on Wiley Online Library for rules of use; OA articles are governed by the applicable Creative Commons License